processes

MDPI

Article

Perforated Spiral-Insert Catalytic Tube for Enhanced CO Catalytic Oxidation: CFD Modeling and Parameter Optimization

Song Dong [1], Dingrui Li [2], Yao Hu [2] and Yanming Wang [3,*]

[1] Shenmu County Longde Mining Co., Ltd., Yulin 719302, China; dsddzyx@163.com
[2] State Key Laboratory of Coal Mine Disaster Prevention and Control, China University of Mining and Technology, Xuzhou 221116, China; tb25120013a41@cumt.edu.cn (D.L.); yao-hu@cumt.edu.cn (Y.H.)
[3] Key Laboratory of Gas and Fire Control for Coal Mines, China University of Mining and Technology, Xuzhou 221116, China
* Correspondence: yanming.wang@cumt.edu.cn

Abstract

To address the challenge of efficient catalytic elimination of carbon monoxide (CO) generated from spontaneous coal combustion in goaf and blasting operations in underground coal mines under low-velocity laminar flow conditions, we propose a perforated spiral-insert catalytic tube. The design inserts a spiral vane with surface micro-holes into a straight tube; the vane surface and internal pore walls are coated with a CuMnOx catalyst. A porous medium equivalent model describes the flow and catalytic reaction characteristics in the perforated region. A three-dimensional Computational Fluid Dynamics (CFD) model coupling flow, mass transfer, and surface catalytic reactions is developed. After grid independence verification, three sets of L9 orthogonal experiments systematically investigate the effects of inlet velocity, helix pitch, vane height, opening ratio, and pore diameter on CO conversion and flow resistance. Range analysis, variance analysis, and the comprehensive performance factor are used for multi-objective optimization. *PEC* results show that inlet velocity is the primary factor affecting both conversion and comprehensive performance, and its dominance is independent of the number of vanes. At a low velocity of 0.2 m/s, the four-vane configuration achieves a maximum conversion of 51.07%. For a balanced trade-off between conversion and flow resistance, four vanes with a high opening ratio, large pore diameter, and large helix pitch yield the best comprehensive performance. If low resistance is the primary goal, two vanes with a high opening ratio achieve a resistance of only 0.29 Pa and a per-unit-resistance conversion efficiency of 97.72 Pa^{-1}. A further predicted optimal combination is validated by simulation, achieving a conversion of 64.96%, confirming the effectiveness of the parameter optimization. Under low-velocity conditions, the flow resistance of this design is only about 0.3–1.3 Pa, allowing passive operation using the natural negative pressure of the extraction pipeline. The design offers modular replaceability of the catalyst insert and operates without external power input beyond the natural negative pressure of the pipeline under the simulated low-velocity conditions, providing a theoretical basis and parameter optimization method for in situ CO catalytic elimination in coal mines.

Keywords: spiral insert tube; CO catalytic oxidation; orthogonal experiment; CFD simulation; parameter optimization; coal mine safety

Check for updates

Academic Editor: Iqbal M. Mujtaba

Received: 18 August 2026
Revised: 2 September 2026
Accepted: 7 September 2026
Published: 9 September 2026

Copyright: © 2026 by the authors. Licensee MDPI, Basel, Switzerland. This article is an open access article distributed under the terms and conditions of the Creative Commons Attribution (CC BY) license.

1. Introduction

Spontaneous coal combustion in goaf and blasting operations in underground coal mines continuously generates large amounts of carbon monoxide (CO), which seriously threatens workers' lives [1,2]. Field data show that coal oxidation in goaf is the main source of CO in the return air corner, where CO concentration can reach 45–96 ppm, with coal oxidation contributing about 78% [1,3,4]. During coal spontaneous combustion, CO concentration in the goaf can reach as high as 3912.6 ppm, far exceeding the allowable limit of 24 ppm specified in the Coal Mine Safety Regulations [5]. Therefore, efficient in situ elimination of CO remains an urgent problem in coal mine safety production.

Current underground CO control methods focus on source suppression and physical dilution, including ventilation dilution, nitrogen injection inertization, inhibitor spraying, and sealing of upper and lower corners [6–8]. However, these methods lack efficient in situ elimination of CO already generated in the goaf. Catalytic oxidation is one of the most economical and effective means of CO elimination: noble metal catalysts offer excellent low-temperature activity and stability, whereas non-noble metal catalysts have cost advantages [9,10]. Among the latter, Cu-Mn composite oxides (CuMnOx/Hopcalite) are the most widely used non-noble metal room-temperature CO oxidation catalysts, and studies have shown that they can achieve complete CO oxidation at room temperature while maintaining high activity for over 250 h [11]. Zhou Fubao's team proposed an active simultaneous treatment method that uses nano-catalyst powder to create an ultra-fine dust cloud that captures and oxidizes CO at the instant of blasting [12], but powder spraying is a consumable active process that cannot achieve long-term continuous operation. Biological metabolism [13] and plasma oxidation [14] have also been attempted, but their adaptability to underground coal mine environments and explosion safety have not been fully verified. In summary, existing CO elimination methods mostly rely on external energy or consumable materials, making it difficult to achieve passive, continuous operation under the long-term unattended conditions of a coal mine.

Passive catalytic solutions that load catalyst onto the inner walls of pipes require no external energy and satisfy intrinsic-safety design intent. However, existing catalytic structures struggle to balance low pressure drop and high mass-transfer efficiency. Catalytic beds provide catalytic area through porous channels formed by particle packing, but their resistance is high, and they are prone to clogging by dust and difficult to replace [15]. For wall-coated or surface-supported catalytic configurations operated under laminar flow, the overall reaction rate can become limited by radial gas-phase mass transfer from the bulk flow to the catalytic surface, thereby restricting effective utilization of the available catalytic area [16]. Compared with these alternatives, the perforated spiral-insert catalytic tube proposed here combines several advantages: it operates passively under the natural negative pressure of the pipeline; the catalyst-bearing insert is modular and replaceable; and it maintains a low pressure drop at low velocity without consumables. Its principal disadvantages and limitations are equally important: the flow model is single-component; the porous-medium equivalence has not yet been directly validated against an explicit perforated geometry; the catalyst is subject to deactivation by H_2S, water vapor, and dust; and scale-up to industrial pipeline diameters has not yet been demonstrated. Achieving efficient CO–catalyst contact under low pressure drop is therefore the core challenge in catalytic structure design.

Spiral inserts such as twisted tapes and helical vanes have long been proven to induce swirl and radial secondary flow in heat exchangers and static mixers, thereby enhancing heat and mass transfer [17,18]. Inspired by perforated twisted tapes for heat transfer enhancement [19,20], we introduce perforations into spiral vanes, which add jet effects through the holes in addition to the swirl flow, further penetrating the near-wall concen-

tration boundary layer and reducing pressure drop across the vane. The novelty of the present work lies in three points: (i) whereas earlier spiral/twisted-insert studies target heat or mass transfer enhancement alone, we use the perforated spiral vane as a catalyst carrier for CO catalytic oxidation, coating both the vane surface and the internal pore walls with CuMnOx; (ii) the insert operates passively under the natural negative pressure of an extraction pipeline, so that no external energy or consumable input is required; and (iii) the perforated region is represented by a porous-medium equivalent model, which makes the densely perforated vane computationally tractable while retaining the jet-driven boundary-layer penetration and the swirl-enhanced convective mass transfer.

Based on this, we propose a perforated spiral-insert catalytic tube and study its CO catalytic oxidation performance through CFD simulation, as shown in Figure 1. A porous medium equivalent model describes the perforated vane region. After grid independence verification for the most geometrically complex case, three sets of L9 orthogonal experiments systematically investigate the effects of inlet velocity, helix pitch, vane height, opening ratio, and pore diameter on CO conversion and pressure drop. Range analysis, variance analysis, and comprehensive performance indicators yield the optimal parameter combination, providing a theoretical basis for engineering application of this technology for in situ CO catalytic elimination in underground coal mine pipelines.

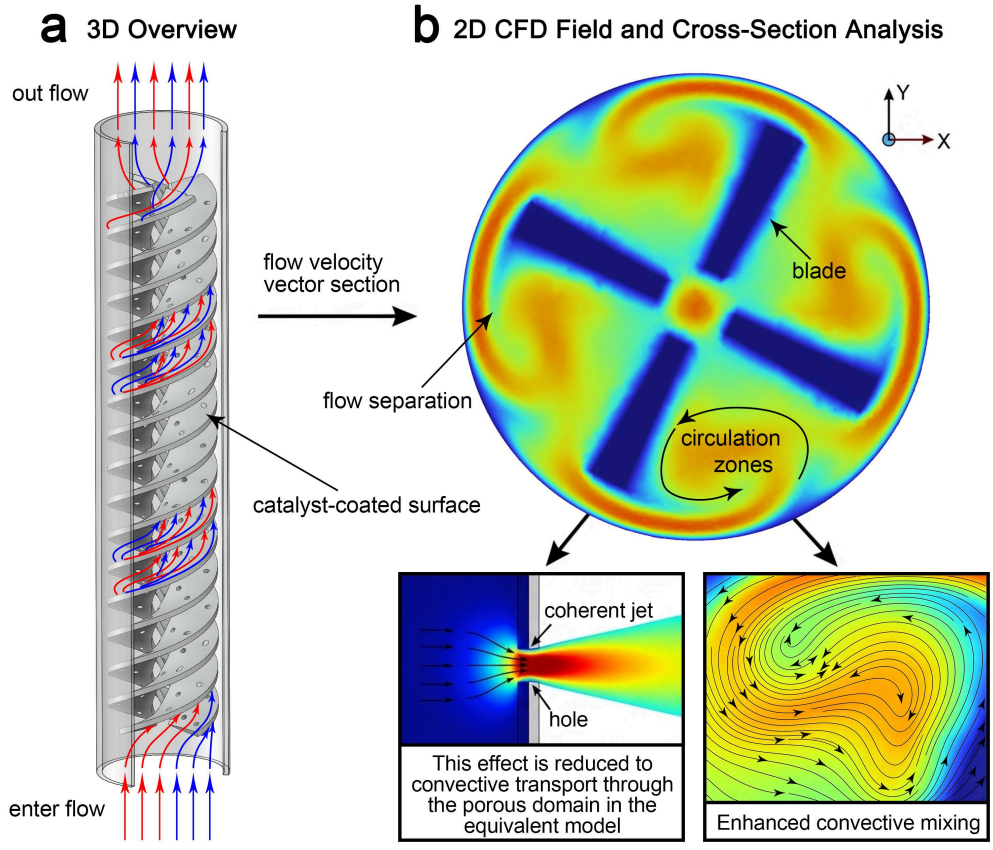


Figure 1. Schematic diagram of perforated spiral-insert catalytic tube structure and mass transfer enhancement mechanism.

In summary, the scope of this study is a three-dimensional CFD investigation of the perforated spiral-insert catalytic tube for CO oxidation under low-velocity laminar flow. The main objectives are (1) to represent the perforated vane region with a porous-medium equivalent model; (2) to conduct three L9(3^5) orthogonal experiments over inlet velocity, helix pitch, vane height, opening ratio, and pore diameter; and (3) to optimize the trade-off between CO conversion, pressure drop, and the comprehensive performance factor.

The specific contributions are the coupled flow–mass transfer–surface catalytic reaction CFD model; the finding that inlet velocity is the dominant factor, independent of the number of vanes; and the optimized configurations for maximum conversion, maximum comprehensive performance, and maximum specific pressure-drop efficiency.

2. Numerical Model and Validation

2.1. Geometric Model

The core functional unit of the perforated spiral-insert catalytic tube is the spiral vane assembly, as shown in Figure 2. The vane extends from the wall toward the center by a certain length, leaving a central vane-free channel. The outer edge of the vane fits and attaches to the inner wall of the extraction pipeline. The catalytic function relies on the CuMnOx catalyst coated on the vane surface and on the internal pore walls. The tube inner wall is inerted and does not participate in catalytic reactions. The vane surface contains regularly distributed micro-holes. To avoid the huge mesh count and computational burden of modeling each hole individually, this study adopts a porous medium equivalent model that describes the flow and catalytic characteristics of the perforated region.

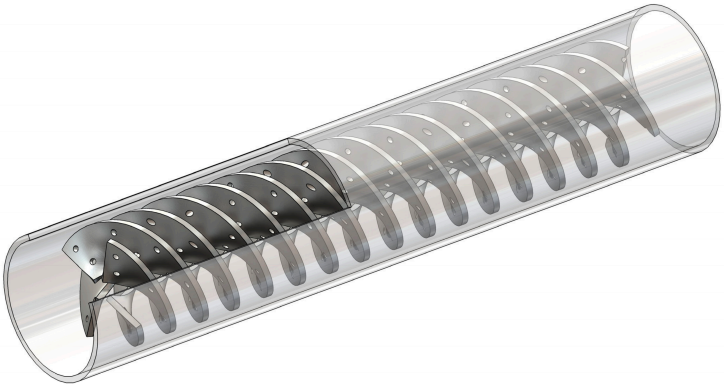


Figure 2. Perforated spiral-insert catalytic tube.

Table 1 lists the main geometric parameters. The baseline parameters are as follows: number of vanes N_{blades} = 4, helix pitch P_{helix} = 20 mm, vane height b_{height} = 8 mm.

Table 1. Geometric parameters.

Parameter	Symbol	Value	Unit
Tube inner diameter	D	20	mm
Inlet straight length	L_{in}	10	mm
Insert length	L_{insert}	100	mm
Outlet straight length	L_{out}	10	mm
Total length	L_{total}	120	mm
Vane thickness	t	1	mm

The baseline reference case is an empty straight tube with catalyst coated on the inner wall and no spiral insert, providing reference pressure drop ΔP_{empty} and reference conversion.

2.2. Porous Medium Equivalent Model

The large number of micro-holes on the vane surface makes modeling each hole individually computationally prohibitive. Because the macroscopic transport effect of the micro-holes primarily manifests as additional flow resistance and permeability, a porous medium equivalent model is used to describe the flow and catalytic reaction

characteristics of the perforated vane region. The vane region is set as a porous domain with porosity ε equal to the opening ratio $open_r$. Permeability κ is determined by the Kozeny–Carman equation:

$$\kappa = \frac{d_{hole}^2 \cdot \varepsilon^3}{180\ (1-\varepsilon)^2} \tag{1}$$

where d_{hole} is the pore diameter.

The effective diffusion coefficient D_{eff} of CO within the porous domain is corrected using the Bruggeman relation:

$$D_{eff} = D_{CO} \cdot \varepsilon^{4/3} \tag{2}$$

The catalytic reaction is applied at two levels: (1) on the external vane surface, using a catalytic consumption flux $R_s = -k_s \cdot c_{CO}$ to simulate the oxidation reaction that occurs when gas contacts the vane surface; (2) inside the porous vane domain, using a volume reaction $R_v = -k_s \cdot a_v \cdot c_{CO}$ to account for the additional catalytic area provided by the internal pore walls, where the specific surface area is $a_v = 4\varepsilon / d_{hole}$.

2.3. Governing Equations and Boundary Conditions

The flow–mass transfer–surface catalytic reaction coupled model is built using COMSOL Multiphysics 6.1. The incompressible Navier–Stokes equations describe the free-flow region, while the Brinkman equations (with permeability given by Equation (1)) describe the porous vane domain.

The steady-state concentration field of CO is described by the convection–diffusion equation:

$$\nabla \cdot (-D\nabla c_{CO}) + \mathbf{u} \cdot \nabla c_{CO} = R \tag{3}$$

where R is the catalytic reaction source term, taking R_s on the external vane surface and R_v inside the porous domain.

Boundary conditions: inlet—fully developed laminar flow and fixed CO concentration (500 ppm, i.e., 7.45×10^{-3} mol/m^3); outlet—zero pressure and outflow boundary; tube inner wall—inert wall. The diffusion coefficient of CO in air D_{CO} = 1.8×10^{-5} m^2/s (25 °C, 1 atm), and the reaction rate constant is taken as k_s = 5×10^{-3} m/s [21]. The selected value is treated as an apparent first-order surface rate constant for the coated CuMnOx layer under the present dilute, isothermal conditions; its influence on the conclusions is checked in Section 4.4.

2.4. Grid Generation and Independence Verification

A physics-controlled adaptive meshing strategy generates progressively refined mesh schemes, resulting in four grids, as shown in Figure 3.

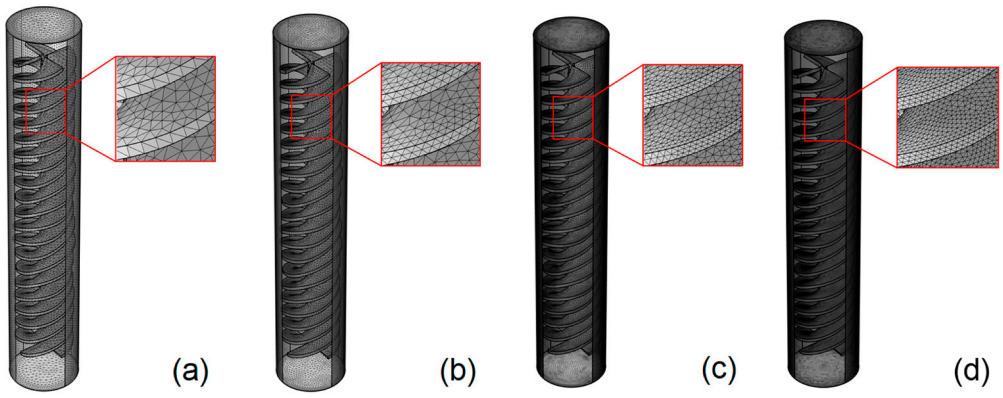


Figure 3. Grids at different refinement levels: (**a**) fine; (**b**) finer; (**c**) extra-fine; (**d**) ultra-fine.

Due to the increase in the number of blades, the flow channel will shrink, and the geometric complexity will significantly increase, requiring higher grid accuracy. Therefore, the grid independence verification is performed conservatively for the most geometrically complex case within the scanning parameter range, i.e., N_{blades} = 4, b_{height} = 8 mm, P_{helix} = 20 mm. CO conversion X and pressure drop ΔP are selected as grid convergence criteria, representing the two core evaluation dimensions of catalytic performance and flow resistance.

Table 2 presents the element counts and corresponding steady-state solutions for the four grids. As the grid refines, both CO conversion and pressure drop decrease monotonically, consistent with the reduction in numerical diffusion. The differences between the extra-fine and ultra-fine grids are 2.9% for CO conversion and 2.4% for pressure drop; these variations are much smaller than those observed with coarser grids. To balance computational efficiency, all subsequent simulations use the extra-fine grid scheme.

Table 2. Grid independence verification results ($N_{blades} = 4$).

Grid Scheme	Element Count	ΔP (Pa)	X (%)
Fine	529,110	2.8835	68.460
Finer	1,649,893	2.4417	64.618
Extra-fine	6,667,684	2.1643	61.192
Ultra-fine	9,527,860	2.1124	59.459

2.5. Model Assumptions

The CFD model in this study is based on the following assumptions:

(1) The gas is an incompressible ideal gas, and the flow is steady-state laminar flow.
(2) The catalytic coating is an ideal uniform surface, and the reaction rate constant k_s is constant, independent of CO concentration and temperature, and its value is taken from [21].
(3) The reaction is simplified to a first-order reaction; the product CO_2 is treated as an inert tracer component, and its influence on flow and catalytic reaction is negligible.
(4) The system is isothermal at 25 °C, neglecting the exothermic effect of CO oxidation.
(5) Only single-component CO catalytic oxidation is considered; the effects of multi-component species such as H_2S, water vapor, and dust present in actual underground conditions are outside the scope of this model.

3. Orthogonal Experimental Design

Five parameters (inlet velocity, helix pitch, vane height, opening ratio, and pore diameter) are selected as factors for the orthogonal experiment, each at three levels, as shown in Table 3. Because the number of vanes involves topological changes, it is treated as a grouping variable. Three separate L9(3^5) orthogonal experiments are conducted for N_{blades} = 2, 3, and 4. The experimental scheme is given in Table 4, totaling 27 cases (3 groups × 9 runs). The experimental design only evaluates the main influencing factors of CO elimination efficiency, without considering the interactions between factors.

Table 3. Factor levels for orthogonal experiment.

Factor	Symbol	Level 1	Level 2	Level 3
Inlet velocity	U_{in}	0.2	0.5	1.0
Helix pitch	P_{helix}	20	30	40
Vane height	b_{height}	6	8	9
Opening ratio	$open_r$	0.1	0.3	0.5
Pore diameter	d_{hole}	2	3	4

Table 4. L9(3^5) orthogonal experimental scheme.

Run	U_{in} (m/s)	P_{helix} (mm)	b_{height} (mm)	$open_r$	d_{hole} (mm)
1	0.2	20	6	0.1	2
2	0.2	30	8	0.3	3
3	0.2	40	9	0.5	4
4	0.5	20	8	0.5	4
5	0.5	30	9	0.1	2
6	0.5	40	6	0.3	3
7	1.0	20	9	0.3	2
8	1.0	30	6	0.5	4
9	1.0	40	8	0.1	3

To comprehensively evaluate the trade-off between catalytic performance and energy cost, the main evaluation indicators are steady-state CO conversion X and pressure drop ΔP. Additionally, the following dimensionless comprehensive indicators are introduced:

$$\eta_{\Delta P} = \frac{X}{\Delta P} \tag{4}$$

$$PEC = \frac{X}{(\Delta P / \Delta P_{empty})^{1/3}} \tag{5}$$

where $\eta_{\Delta P}$ is the specific pressure drop efficiency, reflecting the conversion gain per unit pressure drop; ΔP_{empty} is the pressure drop of an empty straight tube at the same flow velocity; and the comprehensive performance factor PEC balances conversion and pressure drop penalty.

4. Results and Discussion

4.1. Flow Field and Concentration Field Characteristics in Representative Cases

Three representative cases from the orthogonal experiments are selected to compare concentration field distributions with the catalytic empty straight tube, as shown in Figure 4. Case a (N_{blades} = 4, U_{in} = 0.2 m/s, P_{helix} = 30 mm, b_{height} = 8 mm, $open_r$ = 0.3, d_{hole} = 3 mm) achieves the highest conversion (X = 51.07%). Case b (N_{blades} = 4, U_{in} = 0.2 m/s, P_{helix} = 40 mm, b_{height} = 9 mm, $open_r$ = 0.5, d_{hole} = 4 mm) gives the highest comprehensive performance factor PEC (X = 46.43%, ΔP = 0.52 Pa). Case c (N_{blades} = 2, U_{in} = 1.0 m/s, P_{helix} = 30 mm, b_{height} = 6 mm, $open_r$ = 0.5, d_{hole} = 4 mm) yields the lowest conversion (X = 6.71%).

In the catalytic straight tube under laminar flow, CO relies on radial diffusion to reach the catalytic wall, forming a thick concentration boundary layer near the wall. Limited by diffusion mass transfer, the conversion is only 33.31%, and the flow resistance is 0.02 Pa. In the maximum conversion case (four vanes, moderate pitch and opening ratio), the vane-induced helical swirling flow is strongest, compressing the concentration boundary layer most significantly and resulting in the lowest outlet CO concentration. In the maximum PEC case (four vanes, large pitch, high opening ratio), although the swirl intensity is weaker than that in the four-vane moderate case, the flow resistance is only 0.52 Pa, giving the best comprehensive performance. In the minimum conversion case, the high velocity leads to very short residence time, and the limited catalytic area of two vanes leaves the outlet CO concentration close to the inlet concentration, with a conversion of only 6.71%. These comparisons indicate that the dominant factors for conversion are velocity and the number of vanes, while the superiority of comprehensive performance also depends on the magnitude of flow resistance, consistent with the range analysis results of the orthogonal experiments.

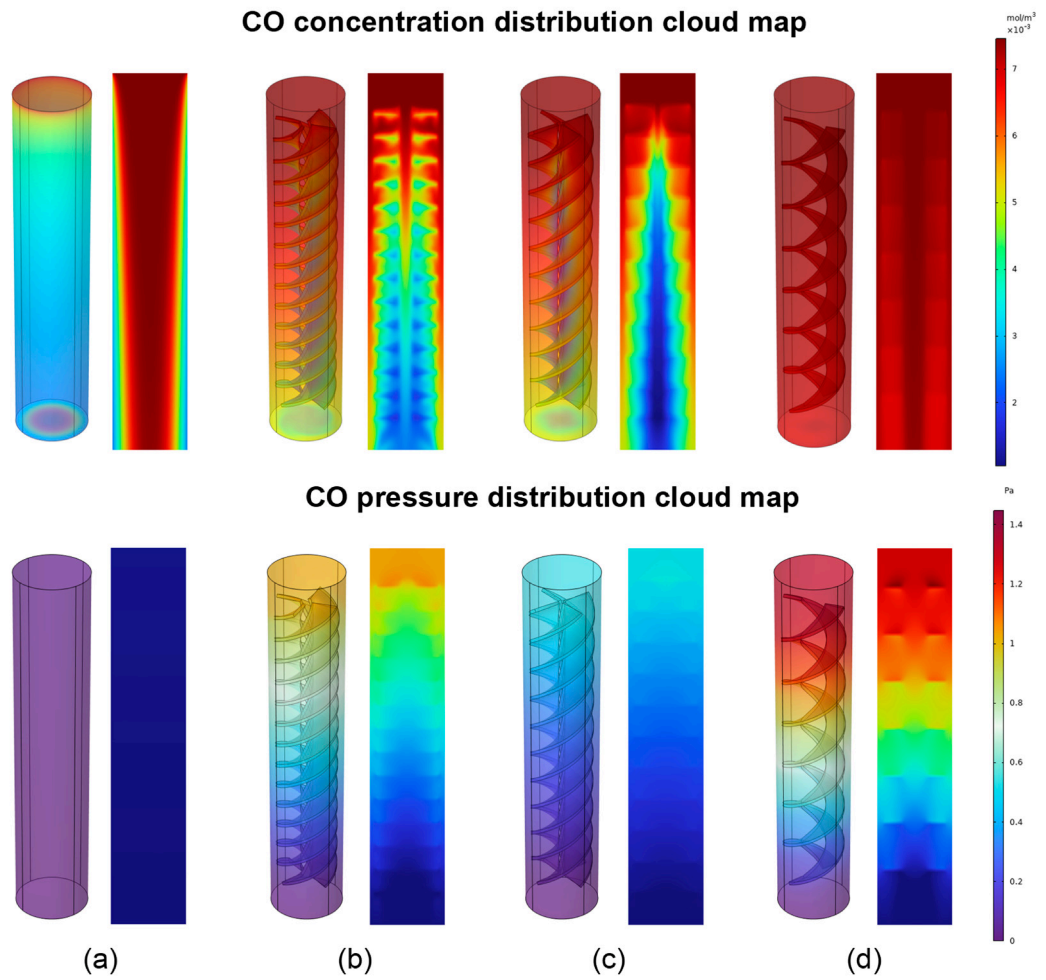


Figure 4. CO concentration and pressure distribution in catalytic straight tube and representative cases: (**a**) catalytic straight tube; (**b**) maximum conversion case; (**c**) maximum *PEC* case; (**d**) minimum conversion case.

4.2. Orthogonal Experiment Results

The CO conversions from the three L9(3^5) orthogonal experiment groups are shown in Figure 5. The highest conversion in all three groups occurs at the low inlet velocity of 0.2 m/s. The four-vane group gives the highest overall conversion, ranging from 48.81% to 51.07%, while the two-vane group at U_{in} = 1.0 m/s gives the lowest conversion, only 6.71%. At the same velocity and geometric parameters, increasing the number of vanes from 2 to 4 monotonically increases conversion; the four-vane configuration yields approximately 1.5 to 1.6 times the conversion of the two-vane configuration.

4.3. Range Analysis and Main Effects

Taking the N_{blades} = 4 group as an example, Table 5 presents the range analysis results for each factor on CO conversion X, and Figure 6 shows the corresponding main effects. A larger range R indicates a more significant influence of that factor on the indicator. Inlet velocity has the largest range (R = 0.2630) and is the primary factor affecting CO conversion. Helix pitch and vane height are secondary (R = 0.1330 and 0.1214, respectively). Pore diameter and opening ratio have relatively smaller influences (R = 0.1144 and 0.0532, respectively).

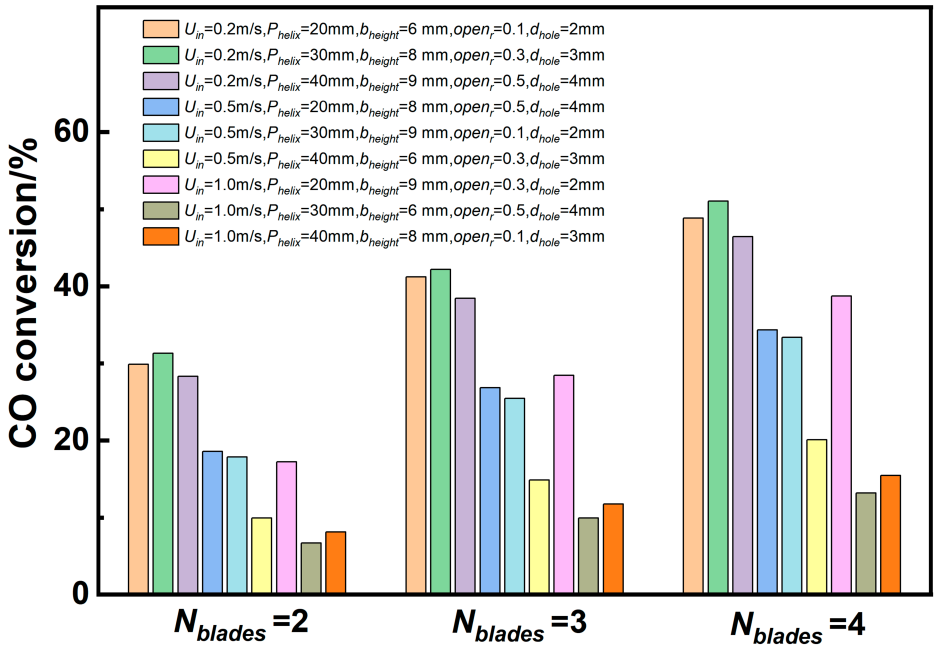


Figure 5. CO conversion in each orthogonal experiment group.

Table 5. Range analysis of factors on conversion (N_{blades} = 4).

Level	A: U_{in}	B: P_{helix}	C: b_{height}	D: $open_r$	E: d_{hole}
K_1	0.4877	0.4063	0.2737	0.3254	0.4031
K_2	0.2927	0.3254	0.3362	0.3664	0.2887
K_3	0.2247	0.2733	0.3951	0.3132	0.3132
R	0.2630	0.1330	0.1214	0.0532	0.1144
Rank	1	2	3	5	4

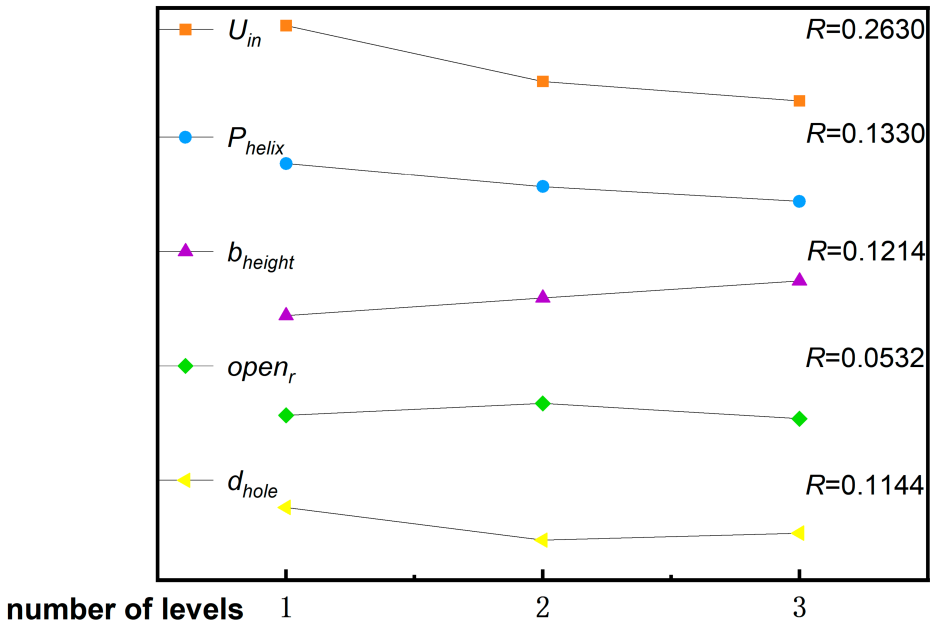


Figure 6. Main effects of factors on CO conversion.

At low velocity, the gas residence time in the catalytic section increases, giving CO more opportunity to diffuse to the vane surface and be catalytically consumed; therefore, K_1 is significantly higher than K_2 and K_3. The K values for pore diameter are lowest at the intermediate level and higher at both ends, indicating a non-monotonic effect: too

small a pore diameter limits gas penetration through the vane to access internal catalytic area, while too large a diameter reduces specific surface area. The K values for helix pitch decrease monotonically with increasing pitch, indicating that more densely spaced vanes enhance swirl intensity and radial secondary flow.

Table 6 summarizes the range ranking for the three vane-number groups. Inlet velocity is the primary influencing factor in all three groups (R = 0.1915–0.2630), and its dominance does not change with the number of vanes. The ranking of secondary factors varies slightly with vane number, but the R values of the last four factors in each group are all within similar ranges.

Table 6. Comparison of range ranking for three vane-number groups.

Rank	N_{blades} = 2	R	N_{blades} = 3	R	N_{blades} = 4	R
1	U_{in}	0.1915	U_{in}	0.2391	U_{in}	0.2630
2	d_{hole}	0.1758	P_{helix}	0.2292	P_{helix}	0.1330
3	P_{helix}	0.1378	d_{hole}	0.1998	b_{height}	0.1214
4	b_{height}	0.0746	$open_r$	0.1127	d_{hole}	0.1144
5	$open_r$	0.0428	b_{height}	0.0927	$open_r$	0.0532

4.4. Variance Analysis

To quantitatively assess the relative importance of each factor, variance analysis is performed on the comprehensive performance factor PEC. Figure 7 summarizes the F-values for the three groups.

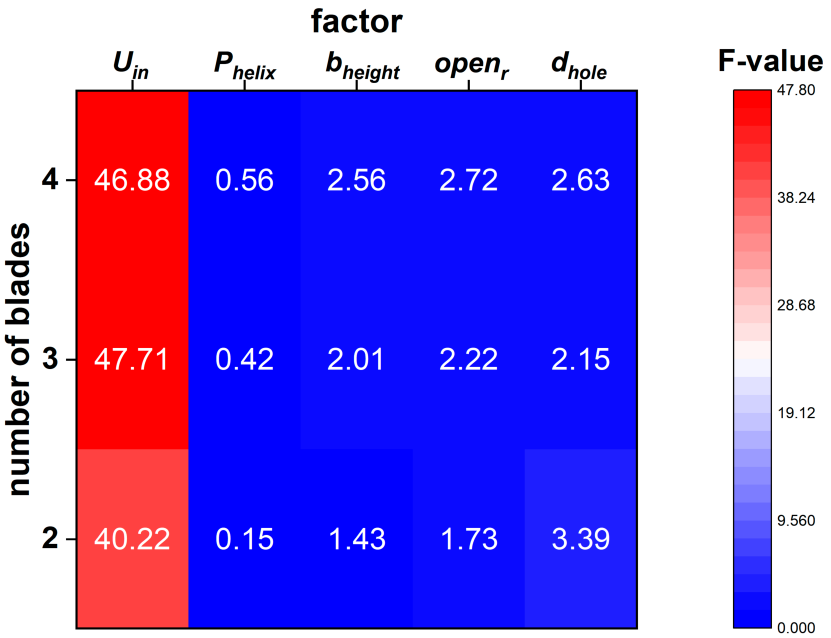


Figure 7. Heatmap of F-values from variance analysis.

Inlet velocity is the only highly significant factor affecting PEC in all three groups, far exceeding the critical value at the 99% confidence level, which is consistent with the conclusions shown in Table 5. For N_{blades} = 2, the F-value for pore diameter is 3.39, which is not significant even at the 90% confidence level but is relatively higher among the five factors. The F-values for helix pitch and vane height are all less than 2.6 in the three groups, indicating statistically insignificant effects on PEC. This means that when pursuing optimal comprehensive performance, apart from the pipeline flow velocity condition, the perforation parameters (i.e., pore diameter and opening ratio) are more critical than the

vane geometric parameters (helix pitch and vane height) because the former directly affect flow resistance, while the latter mainly influence the swirl structure and catalytic area.

Because the adopted surface reaction rate constant $k_s = 5 \times 10^{-3}$ m/s is a key model input, a local sensitivity check was added for the predicted optimal configuration ($N_{blades} = 4$, $U_{in} = 0.2$ m/s, $P_{helix} = 20$ mm, $b_{height} = 9$ mm, $o_r = 0.3$, $d_{hole} = 2$ mm), as shown in Table 7. Keeping the flow field and geometric parameters unchanged, ks was varied by ±50%. The apparent first-order response gives conversions of 40.82%, 64.96%, and 79.29% for $0.5k_s$, k_s, and $1.5k_s$, respectively, while the pressure drop remains 2.09 Pa because the hydrodynamic equations are not coupled to the dilute CO consumption term. Thus, k_s strongly affects the absolute conversion level but does not change the pressure-drop ranking or the conclusion that inlet velocity is the dominant factor in the orthogonal analysis.

Table 7. Sensitivity of predicted optimal performance to the apparent surface reaction rate constant k_s.

Case	k_s (m/s)	Relative k_s	CO Conversion X (%)	Pressure Drop ΔP (Pa)	Interpretation
Low-activity check	2.5×10^{-3}	0.5	40.82	2.09	Conversion decreases, but the same geometry remains governed by residence time and pressure-drop trade-off.
Nominal model	5.0×10^{-3}	1.0	64.96	2.09	Baseline predicted optimum validated by CFD in Section 4.5.
High-activity check	7.5×10^{-3}	1.5	79.29	2.09	Conversion increases, while hydrodynamic resistance and factor ordering remain unchanged.

4.5. Comprehensive Performance Evaluation and Optimal Parameters

Table 8 lists the optimal parameter combinations for the three optimization objectives: conversion X, specific pressure drop efficiency $\eta_{\Delta P}$, and comprehensive performance factor PEC. The optimal parameters differ among the three objectives. Achieving maximum conversion requires four vanes and a moderate opening ratio. Achieving maximum $\eta_{\Delta P}$ requires two vanes with a high opening ratio, large pore diameter, and large helix pitch. Achieving maximum PEC requires four vanes with a high opening ratio, large pore diameter, and large helix pitch. These differences reflect the trade-off between conversion and flow resistance: the maximum conversion scheme has the highest resistance, the maximum $\eta_{\Delta P}$ scheme gives the lowest conversion but extremely low resistance, and the maximum PEC scheme achieves the best balance between the two.

This difference indicates that in practical engineering design, the trade-off between conversion and flow resistance must be weighed against specific requirements. If the pipeline driving pressure head is ample, the four-vane scheme can be used to pursue high conversion. If low resistance and long-term operational reliability are the primary goals, the two-vane-with-high-opening-ratio scheme is more suitable. In practical terms, where the pipeline negative-pressure head is ample, the maximum-conversion (four-vane) scheme maximizes CO removal; where long-term passive operation and minimum flow resistance matter (low-pressure-head, unattended, dust-prone conditions), the maximum-PEC scheme is preferable because it accepts a small conversion loss in exchange for a significant pressure drop.

Table 8. Comparison of optimal parameter combinations for different optimization objectives.

Indicator	Max X	Max $\eta_{\Delta P}$	Max PEC
N_{blades}	4	2	4
U_{in} (m/s)	0.2	0.2	0.2
P_{helix} (mm)	30	40	40
b_{height} (mm)	8	9	9
$open_r$	0.3	0.5	0.5
d_{hole} (mm)	3	4	4
X (%)	51.07	28.34	46.43
ΔP (Pa)	1.02	0.29	0.52
$\eta_{\Delta P}$ (Pa^{-1})	50.07	97.72	89.29
PEC	0.1463	0.1234	0.1665

To further explore whether a better combination exists in the parameter space, we propose a parameter combination predicted to maximize conversion (N_{blades} = 4, U_{in} = 0.2 m/s, P_{helix} = 20 mm, b_{height} = 9 mm, $open_r$ = 0.3, d_{hole} = 2 mm) using level-by-level main-effect selection guided by the range analysis and the ANOVA trends, followed by a confirmatory CFD calculation within the discrete factor levels listed in Table 3. CFD simulation validates this combination, yielding a conversion of 64.96%, which is higher than the current optimal value of 51.07%, with a flow resistance of 2.09 Pa. This combination lies within the investigated levels of Table 3, so the 64.96% result is a prediction inside the scanned parameter space rather than a value outside it, and it improves on the best orthogonal case (51.07%) chiefly because the smaller pitch (20 mm) increases vane surface density and swirl, the larger vane height (9 mm) increases catalytic area, and the smaller pore diameter (2 mm) increases specific surface area, at the cost of higher resistance (2.09 Pa).

4.6. Discussion

The orthogonal experiment and comprehensive performance evaluation results systematically reveal the influence of each parameter on the CO elimination performance of the perforated spiral-insert catalytic tube. Inlet velocity, by altering gas residence time and secondary flow intensity, is the primary factor affecting conversion. This conclusion is consistent with the mass-transfer-controlled mechanism of laminar catalytic reactions: at low velocity, CO has more time to diffuse to the catalytic surface, while the secondary flow intensity is weaker; the combined effect of mass transfer enhancement and residence time determines the trend of conversion with velocity. The number of vanes and vane height mainly affect mass transfer by changing the catalytic area and swirl structure. The perforation parameters (pore diameter and opening ratio) have a smaller marginal effect on conversion, but their F-values relative to PEC are larger than those of vane geometric parameters. In fact, large pore diameter and high opening ratio sacrifice a small amount of catalytic area, but the benefit from drastically reducing flow resistance far outweighs this loss, thus establishing superior comprehensive energy efficiency.

From an engineering application perspective, the perforated spiral-insert catalytic tube shows significant advantages under low-velocity conditions: at 0.2 m/s, the flow resistance is on the order of only about 0.3–1.3 Pa, allowing passive operation using the natural negative pressure of the goaf extraction pipeline without additional power. The catalytic function is fully integrated into the replaceable spiral insert, while the tube remains an inert flow channel. When the catalyst deactivates after long-term operation, only the insert needs to be replaced, resulting in low maintenance costs.

This study has the following limitations. First, the porous medium equivalent model has not been directly calibrated against experimental data from real perforated vanes

or metal foams. The Kozeny–Carman permeability and Bruggeman effective-diffusivity corrections capture only the macroscopic added resistance and transport of the hole array, and cannot resolve hole-by-hole jetting, near-hole velocity gradients, or edge effects; the predicted conversion and pressure drop are therefore sensitive to the assumed porosity (=opening ratio) and pore diameter, which are themselves targets of the optimization. Direct validation against a real perforated vane, a metal foam, or an explicit micro-pore geometry should compare the porous-medium and resolved-hole predictions for conversion and pressure drop under the same inlet velocity, opening ratio, and pore diameter; this is required before the absolute conversion values are used for design, and this is flagged as future work. Second, only single-component CO catalytic oxidation is considered. H_2S can act as a catalyst poison, water vapor can compete for active sites and reduce low-temperature activity, and dust can physically block pores and the catalytic surface, all of which would lower conversion and shorten catalyst life relative to the clean single-component predictions. The reported conversions therefore represent an upper-bound estimate for clean CO–air conditions, and multi-component CFD with poisoning and deactivation kinetics is required before the values are applied to real mine gas. Third, the simulations are performed only for a 20 mm diameter tube, whereas industrial extraction pipelines are typically 200–300 mm in diameter. The flow regime and residence-time scaling must be re-verified at industrial diameter and length; the porous-medium permeability and near-wall mass-transfer enhancement are functions of pore size relative to tube diameter and do not scale linearly; and the manufacturing and dust-management constraints differ at pipeline scale. The present results therefore provide a qualitative design basis and an optimization method rather than directly transferable quantitative design values, and prototype tests at industrial scale are required. These issues will be addressed in future work through multi-component CFD simulations and prototype experiments.

5. Conclusions

(1) This paper proposes a perforated spiral-insert catalytic tube that integrates the entire catalytic function into a replaceable spiral insert, leaving the tube as an inert flow channel. A porous medium equivalent model describes the flow and catalytic reaction characteristics of the perforated vane. CFD simulations confirm that the helical swirl flow and radial secondary flow induced by the vane effectively compress the concentration boundary layer and enhance convective mass transfer of CO toward the catalytic wall.

(2) Grid independence is verified for the most geometrically complex case with four vanes. The differences between the ultra-fine and extra-fine grids are about 2.9% for CO conversion and 2.4% for pressure drop, confirming that the extra-fine grid scheme meets accuracy requirements and is applicable to all scanning parameters. Three L9 orthogonal experiments systematically investigate the effects of five factors (inlet velocity, helix pitch, vane height, opening ratio, and pore diameter) on CO conversion and flow resistance.

(3) Range analysis and variance analysis consistently show that inlet velocity is the primary factor affecting both CO conversion and the comprehensive performance factor PEC, and its dominance is independent of the number of vanes. The other four factors have statistically insignificant effects on PEC, but the F-values of pore diameter and opening ratio are clearly higher than those of helix pitch and vane height, indicating that perforation parameters have a greater influence on comprehensive performance than vane geometric parameters.

(4) The optimal parameter combinations for the three optimization objectives differ. The maximum-conversion scheme increases conversion from 33.31% (catalytic straight

tube) to 51.07%. The maximum-PEC scheme achieves the best balance between conversion and flow resistance, with PEC = 0.1665. The maximum-$\eta_{\Delta P}$ scheme yields an extremely low flow resistance of 0.29 Pa and a per-unit-resistance conversion efficiency of 97.72 Pa^{-1}. A predicted optimal combination is validated by CFD, achieving a conversion of 64.96%, further demonstrating the effectiveness of parameter optimization.

(5) Under low-velocity conditions, the flow resistance of the perforated spiral-insert catalytic tube is on the order of only about 0.3–1.3 Pa, allowing passive operation using the natural negative pressure of the extraction pipeline. Within the modeled passive configuration and the simulated low-velocity conditions, the design requires no external power input beyond the natural negative pressure of the extraction pipeline, and it contains no ignition source or moving powered parts, which is consistent with intrinsic-safety design intent but is not demonstrated by this simulation. Together with modular replaceability of the catalyst insert, this provides a new technical solution for in situ catalytic elimination of CO in confined spaces of underground coal mines.

Author Contributions: Conceptualization, methodology, Y.W.; software, writing—original draft preparation, investigation, S.D.; validation, writing—review and editing, D.L.; visualization, formal analysis, Y.H. All authors have read and agreed to the published version of the manuscript.

Funding: This research received no external funding.

Data Availability Statement: The data that support the findings of this study are available on request from the corresponding author. The data are not publicly available due to privacy or ethical restrictions.

Conflicts of Interest: Author Song Dong was employed by the Shenmu County Longde Mining Co., Ltd. The remaining authors declare that the research was conducted in the absence of any commercial or financial relationships that could be construed as potential conflicts of interest.

References

1. Liang, Y.T.; Zhang, P.C.; Sun, Y.; Jia, B.S.; Zhang, D.P.; Guo, B.L. Research on the influence of air leakage velocity on the oxidation behavior of residual coal in the goaf. *Coal Sci. Technol.* **2025**, *53*, 167–179.
2. Liang, Y.T.; Luo, H.Z. Current situation and development trend for coal mine fire prevention & extinguishing techniques in China. *J. China Coal Soc.* **2008**, *33*, 126–130.
3. Zhang, R. Research on CO Migration Law and Its Prevention and Control Technology in the Goaf of Shaping Coal Mine. Master's Thesis, Liaoning Technical University, Fuxin, China, 2023.
4. Li, L. Research and control technology of oxidation co production at normal temperature in Chahasu Coal Mine. *China Energy Environ. Prot.* **2022**, *44*, 40–45+57.
5. Qin, B.T.; Gao, Y.; Shi, Q.L.; Shi, G.Q. Comprehensive prevention and control technology of coal spontaneous combustion in compound goaf of close distance coal seam. *Ind. Mine Autom.* **2021**, *47*, 1–6.
6. Li, C.Y.; Zhou, C.S.; Zhang, Y.L.; Qi, J.L. Analysis of CO sources and the control measures for CO overrun in fully mechanized mining face of shallow contiguous coal seams. *Coal Eng.* **2025**, *57*, 85–91.
7. Kang, Y.L.; Zhao, Y.M.; Shi, J.L. Optimization and application of CO absorbent for coal mine. *China Coal* **2022**, *48*, 41–45.
8. Dou, B.L.; Wang, Z.L. Practice of controlling abnormal CO emission in closed goaf of coal mine. *China Energy Environ. Prot.* **2020**, *42*, 30–33.
9. Dai, X.; Ren, D.Z.; Guo, L.; Zhu, J.F.; Yu, F.; Chang, S.Y. The progress of noble metal catalysts for low-temperature catalytic oxidation of carbon monoxide. *J. Funct. Mater.* **2024**, *55*, 1060–1067.
10. Peng, Z.J.; Wang, T.; Cheng, Y.H.; Wang, X.M.; Zhang, M.; Liu, Y.X.; Xue, Y.; Liu, B.F. Research progress on catalysts for CO oxidation elimination. *Ind. Catal.* **2024**, *32*, 14–22.
11. Grifasi, N.; Sartoretti, E.; Legutko, P.; Bensaid, S.; Russo, N.; Adamski, A.; Fino, D.; Piumetti, M. Copper-manganese oxide catalysts for low-temperature oxidation of indoor pollutants. *Appl. Catal. B Environ. Energy* **2026**, *385*, 126292. [CrossRef]

12. He, S.; Gao, S.; Li, J.; He, S.; Yu, Y.; Wu, J.; Wang, X.; Wang, G.; Chen, X.; Zhou, F. Research on an in-situ synchronous CO elimination method in blasting operations and engineering experimental application based on nano-CO catalysts. *J. Environ. Chem. Eng.* **2024**, *12*, 113260. [CrossRef]
13. Wang, C.P.; Zhang, Y.; Deng, Y.; Duan, X.D.; Wang, J.R.; Wang, N.; Zheng, S.Y. Biodegradation characteristics of CO gas in coal mine goaf using biological methods. *J. Xi'an Univ. Sci. Technol.* **2025**, *45*, 704–715.
14. Zhai, X.W.; Wang, J.G.; Song, B.B.; Zhou, Y.J. Experimental study of CO elimination law by plasma. *Coal Eng.* **2024**, *56*, 254–259.
15. Zamaniyan, A.; Mortazavi, Y.; Khodadadi, A.A.; Manafi, H. Tube fitted bulk monolithic catalyst as novel structured reactor for gas–solid reactions. *Appl. Catal. A Gen.* **2010**, *385*, 214–223. [CrossRef]
16. Aguirre, A.; Chandra, V.; Peters, E.A.J.F.; Kuipers, J.A.M.; D'Angelo Neira, M.F. Open-cell foams as catalysts support: A systematic analysis of the mass transfer limitations. *Chem. Eng. J.* **2020**, *393*, 124656. [CrossRef]
17. Abushammala, O.; Hreiz, R.; Lemaître, C.; Favre, É. Optimal design of helical heat/mass exchangers under laminar flow: CFD investigation and correlations for maximal transfer efficiency and process intensification performances. *Int. J. Heat Mass Transf.* **2020**, *153*, 119610. [CrossRef]
18. Abushammala, O.; Hreiz, R.; Lemaître, C.; Favre, É. Heat and/or mass transfer intensification in helical pipes: Optimal helix geometries and comparison with alternative enhancement techniques. *Chem. Eng. Sci.* **2021**, *234*, 116452. [CrossRef]
19. Bhuiya, M.M.K.; Chowdhury, M.S.U.; Saha, M.; Islam, M.T. Heat transfer and friction factor characteristics in turbulent flow through a tube fitted with perforated twisted tape inserts. *Int. Commun. Heat Mass Transf.* **2013**, *46*, 49–57. [CrossRef]
20. Eiamsa-ard, S.; Wongcharee, K.; Eiamsa-ard, P.; Thianpong, C. Heat transfer enhancement in a tube using delta-winglet twisted tape inserts. *Appl. Therm. Eng.* **2010**, *30*, 310–318. [CrossRef]
21. Dey, S.; Dhal, G.C.; Mohan, D.; Prasad, R. Study of Hopcalite (CuMnOx) catalysts prepared through a novel route for the oxidation of carbon monoxide at low temperature. *Bull. Chem. React. Eng. Catal.* **2017**, *12*, 393–407. [CrossRef]

Disclaimer/Publisher's Note: The statements, opinions and data contained in all publications are solely those of the individual author(s) and contributor(s) and not of MDPI and/or the editor(s). MDPI and/or the editor(s) disclaim responsibility for any injury to people or property resulting from any ideas, methods, instructions or products referred to in the content.